nature geoscience

SUPPLEMENTARY INFORMATION

https://doi.org/10.1038/s41561-018-0111-y

In the format provided by the authors and unedited.

Oxygenation of the Mesoproterozoic ocean and the evolution of complex eukaryotes

Kan Zhang[1,2], Xiangkun Zhu[1]*, Rachel A. Wood[3], Yao Shi[1], Zhaofu Gao[1] and Simon W. Poulton[2]

[1]MLR Key Laboratory of Isotope Geology, MLR Key Laboratory of Deep-Earth Dynamics, Institute of Geology, Chinese Academy of Geological Sciences, Beijing, China. [2]School of Earth and Environment, University of Leeds, Leeds, UK. [3]School of Geosciences, University of Edinburgh, Edinburgh, UK.
*e-mail: xiangkunzhu@163.com

Oxygenation of the Mesoproterozoic ocean and the evolution of complex eukaryotes

Supplementary Information

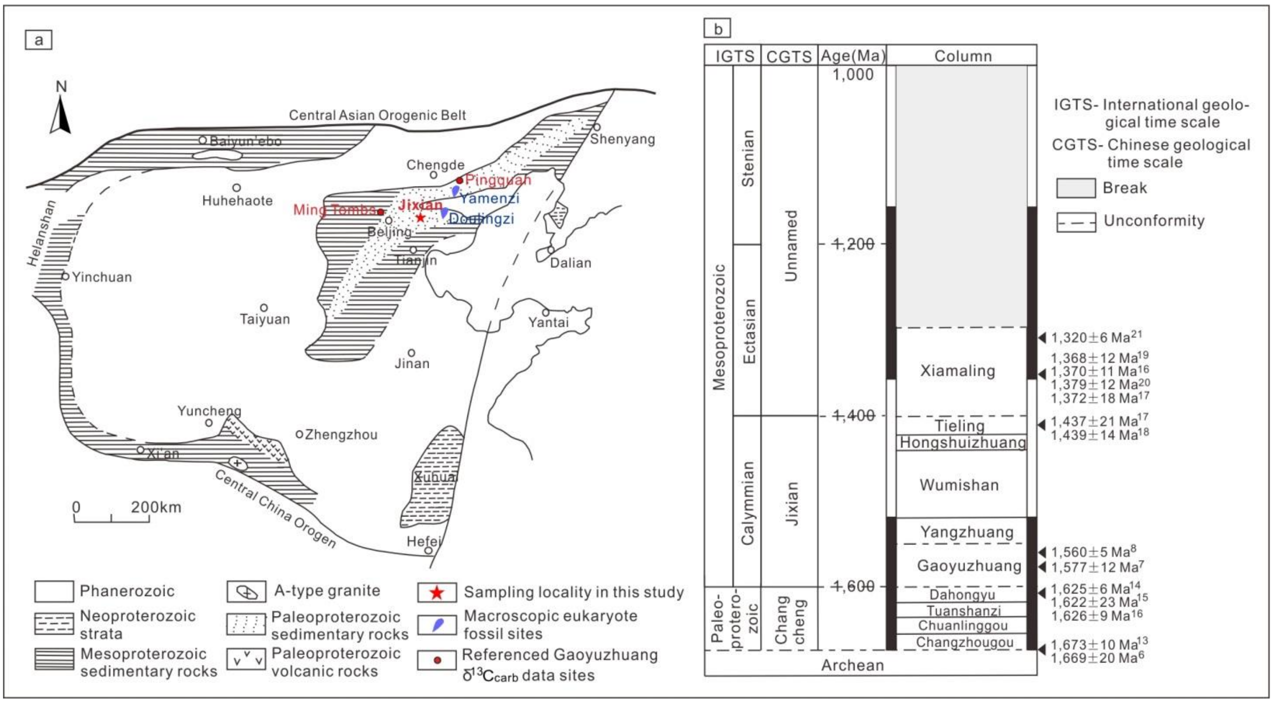

Supplementary Figure 1: (a) Simplified geologic map showing the Proterozoic sedimentary distribution in North China Craton (modified from ref 1). Yanliao Basin is developed at the margin of the eastern block of the North China Craton. Our samples were collected from the Gaoyuzhuang Formation in Jixian Section, Yanliao Basin. The Gaoyuzhuang Formation is divided into four lithological members from bottom up: Guandi Member (GYZ-1), Sangshu'an Member (GYZ-2), Zhangjiayu Member (GYZ-3) and Huanxiusi Member (GYZ-4). Macroscopic eukaryote fossils were discovered in the same basin, which were collected from the Zhangjiayu Member of the Gaoyuzhuang Formation at Doulingzi village, Qianxi and Yamenzi village, Kuancheng[2]. The carbon isotope data ($\delta^{13}C_{carb}$) of Gaoyuzhuang Formation from Pingquan Section[3] and Ming Tombs Section[4] are referenced for comparison in this study. (b) The stratigraphic division of Late-Paleoproterozoic -Mesoproterozoic in Yanliao Basin, North China Craton[5,6]. The depositional age of the Gaoyuzhuang Formation is in the time span of ca. 1,600-1,550 Ma[7,8].

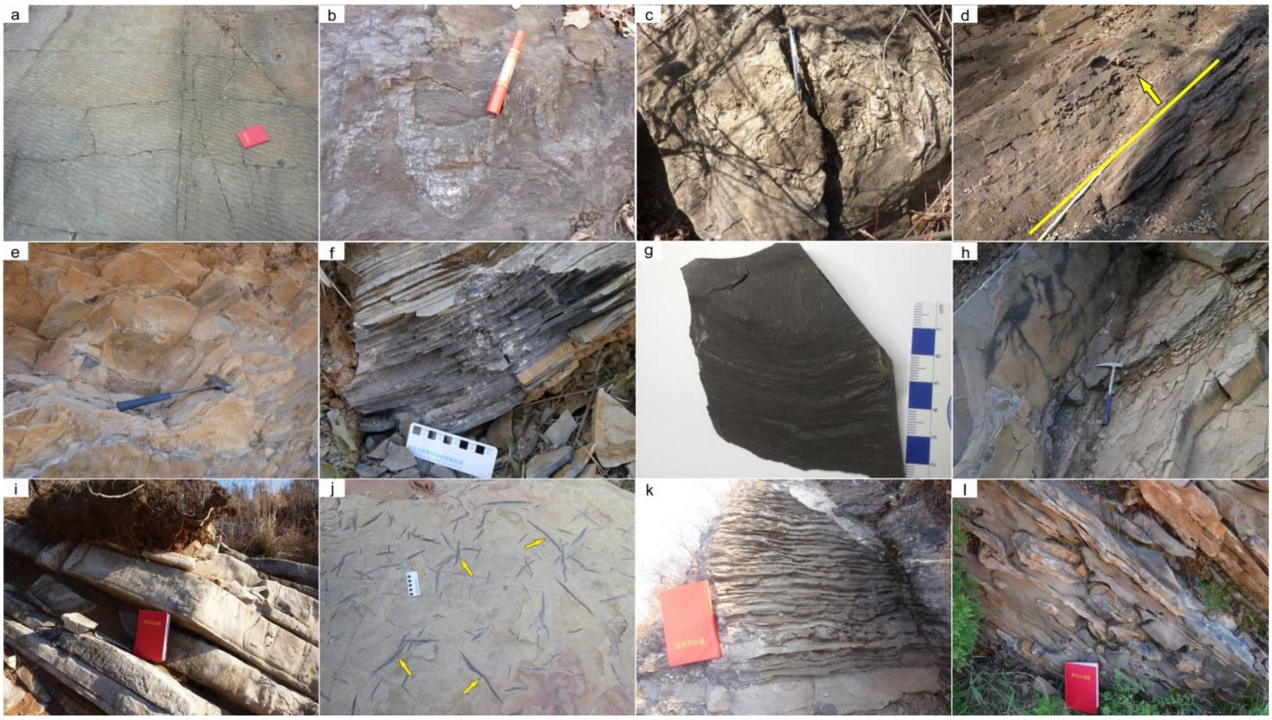

Supplementary Figure 2: Field photographs and hand specimens showing the sedimentary facies of the Gaoyuzhuang Formation in Jixian Section. (a) Quartz sandstone with ripple-marks on the surface at the bottom of GYZ-1. (b) Silicified microbial mats in GYZ-1. (c) Wavy microbial mats in GYZ-1. (d) The contact between GYZ-1 and GYZ-2, below the yellow line is cherty dolostone at the top of GYZ-1; above is thinly bedded clay-rich dolomicrite intercalated with dolomitic siltstone at the bottom of GYZ-2. (e)-(h) Nodular limestones, thin and horizontally-bedded limestones without current-influenced structures, finely laminated carbonates, muddy dolostone and shale in the lower interval of GYZ-3, reflecting deep water facies which may be below storm wave base. (i) Planar beds of limestone and dolomitic limestone in the upper interval of GYZ-3. (j) Molar tooth limestone in the upper interval of GYZ-3. (k) Stromatolitic bioherm in the lower part of GYZ-4. (l) Dolostone with cherty concretions or beds in the upper interval of GYZ-4.

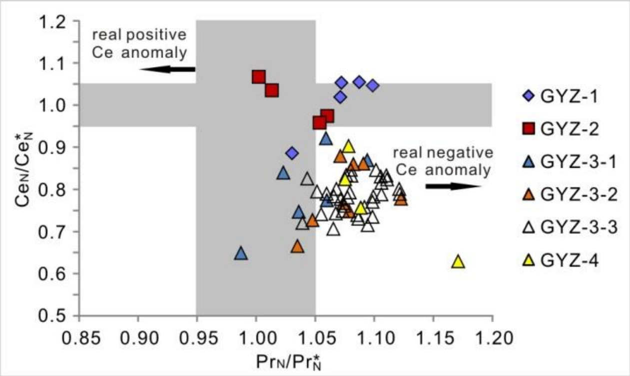

Supplementary Figure 3: Plots of PAAS-normalized Pr_N/Pr^*_N ($Pr_N/(0.5Ce_N+0.5Nd_N)$) versus Ce_N/Ce^*_N ($Ce_N/(0.5La_N+0.5Pr_N)$) using the method of ref 9. This plot discriminates between La and Ce anomalies.

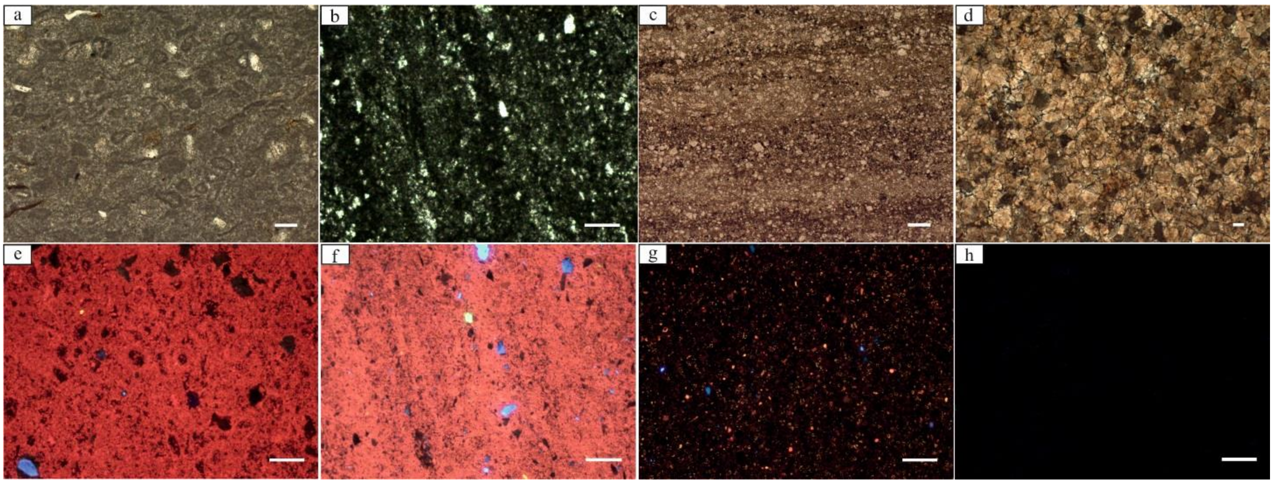

Supplementary Figure 4: Photomicrographs of carbonates from the Gaoyuzhuang Formation, Jixian Section. (a)-(c): Optic features under plane polarized light; (d): Optic features under cross-polarized light; (e)-(h): Corresponding cathodoluminescent images of (a)-(d) respectively. (a) Packstone dolostones from GYZ-1, showing very well-preserved coated grains and micrite matrix. (b) Micritic dolostone with angular quartz grains and possible algal laminae from GYZ-2. (c) Laminated micrite with small scattered euhedral or subhedral dolomites from GYZ-3. (d) Sparitic, recrystallized dolostone from GYZ-4 showing unimodal, nonplanar texture. (e) Grains showing early dolomite replacement with no widespread recrystallisation; Non-luminescent carbonate grains and bright cements; fabric-retentive features are preserved. (f) Non-luminescent carbonate grains with bright luminescent cements. (g) Non-luminescent micrite matrix with many very small zoned early replacive dolomites with a dull luminescent core and bright luminescent rim. (h) Non-luminescent sparry dolostone. White bar in each image represents 100 μm.

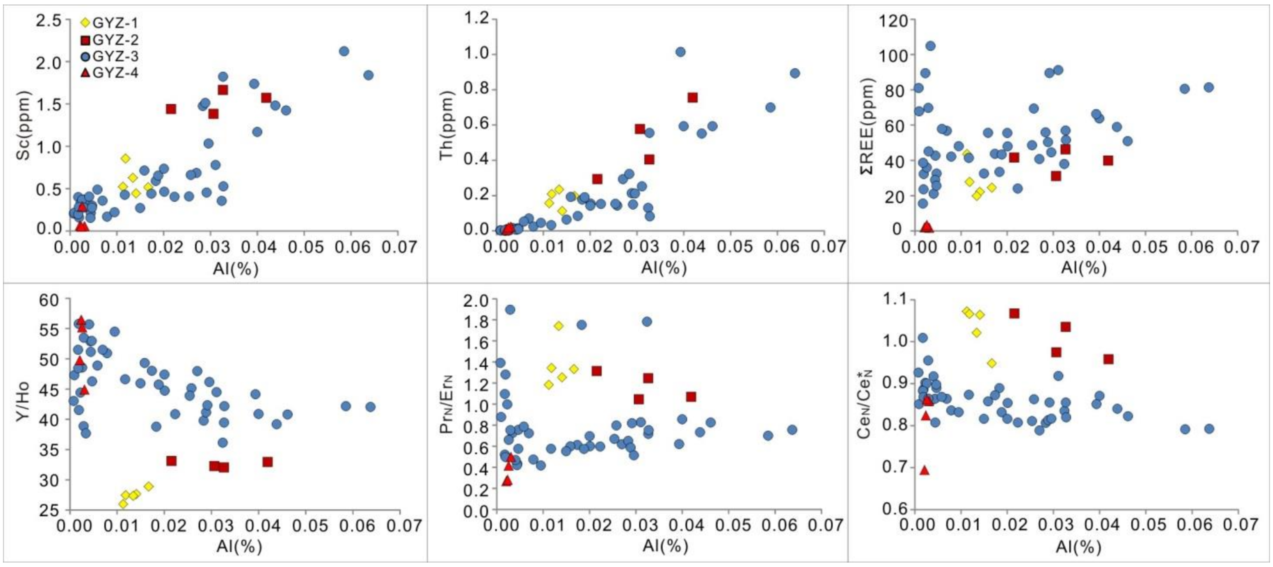

Supplementary Figure 5: Cross-plots of Al-Sc, Al-Th, Al-ΣREE (the sum of REEs), Al-Y/Ho, Al-Pr_N/Er_N (the fractionation between light REE and heavy REE) and Al-Ce_N/Ce_N^* (Ce anomaly) in carbonate leaches of Gaoyuzhuang Formation, Jixian Section. Elements such as Al, Sc, Th are usually used as indicators of detrital materials since they are abundant in these minerals. For our samples, broad positive correlations exist among Al, Th, Sc of carbonate leachates. However, no correlations between Al and ΣREE, Al and Y/Ho, Al and Pr_N/Er_N, or Al and Ce_N/Ce_N^* are observed, suggesting that the possibility of terrigenous contamination can be excluded.

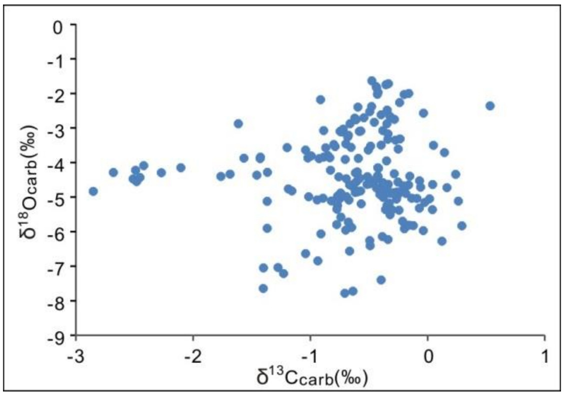

Supplementary Figure 6: Cross-plots of $\delta^{13}C_{carb}$-$\delta^{18}O_{carb}$ in whole carbonate samples of the Gaoyuzhuang Formation, Jixian Section.

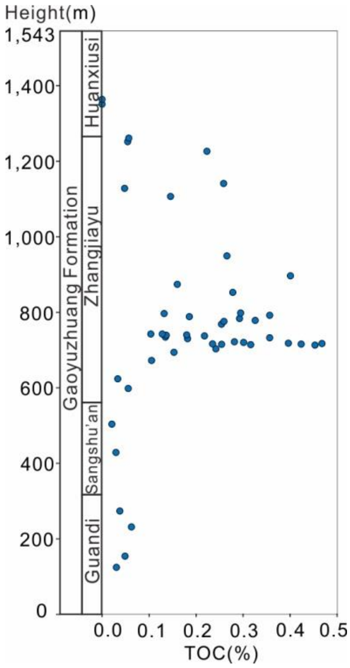

Supplementary Figure 7: Total organic carbon (TOC) profile for carbonates of the Gaoyuzhuang Formation, Jixian Section.

Supplementary Note 1: Geological background

1.1 Regional geology

The Yanliao Basin represents an intracontinental rift basin that developed on the margin of the eastern block of the North China Craton about 1.8 billion years ago (Supplementary Fig. 1a), which is potentially associated with the breakup of the supercontinent Columbia[1,10]. A ca.

9-km-thick succession of Proterozoic sedimentary rocks were deposited atop an Archean-Paleoproterozoic crystalline basement in this basin, and the most complete Proterozoic stratigraphic succession is best exposed in the Jixian region, 100 km east of Beijing, which serves as a significant type section in China. In ascending order, the Jixian Section is divided into: (1) The Changcheng Group (1,650-1,600 Ma), consisting of the Changzhougou, Chuanlinggou, Tuanshanzi and Dahongyu Formations; (2) The Jixian Group (1,600-1,400 Ma), consisting of the Gaoyuzhuang, Yangzhuang, Wumishan, Hongshuizhuang and Tieling Formations; (3) An unnamed group (1,400-1,000 Ma), containing a single stratigraphic unit – the Xiamaling Formation (the upper strata are absent) [5,6]; (4) The Qingbaikou Group (1,000-800 Ma), consisting of the Changlongshan and Jing'eryu Formations (Supplementary Fig. 1b). The Changcheng Group represents the initial development of the Yanliao Basin. Sediments deposited during this stage consist mainly of sandstone and shale, with small amounts of dolostone in the upper part. The volcanic rocks in the Tuanshanzi and Dahongyu Formations mark the highest peak of development of the basin. The Jixian Group records near continuous marine deposition within the Yanliao Basin. Since the Gaoyuzhuang Period, the basin became gradually more stable, but still involved differential subsidence, developing an epeiric sea environment with apparent access to the open ocean. The maximum transgression took place in the Gaoyuzhuang Period, which also established the maximum extent of this epeiric sea. Thick marine carbonate rocks were deposited from the Gaoyuzhuang to Wumishan Period, especially in the Jixian area, the depocenter, where approximately 5,700 m thickness of carbonates were deposited. After this, thin sandstone-shale-carbonate rocks with little facies variability developed (Hongshuizhuang to Xiamaling Formations). The Qingbaikou Group, which mainly consists of sandstone and shale, marks the return of dominantly siliciclastic deposition prior to regional uplift of the Yanliao Basin[11,12].

1.2 Geochronological framework

A high-precision chronological framework has been established for the Proterozoic strata exposed in North China Craton in recent years (Supplementary Fig. 1b). The base age of the Changcheng Group is younger than 1,670 Ma, probably close to 1,650 Ma on the basis of zircon U-Pb ages of 1,673±10 Ma (using LA-MC-ICPMS)[13] and 1,669±20 Ma (using SHRIMP)[6] obtained from a granite-porphyry dike that is overlain unconformably by the Changzhougou Formation. Zircon U-Pb ages of 1,625±6 Ma[14], 1,622±23 Ma[15], and 1,626±9 Ma[16] have been reported for the volcanic rocks collected from the upper part of the Dahongyu Formation. In addition, Li et al. (2010) obtained two almost identical zircon U-Pb ages of 1,559±12 Ma (using SHRMP) and 1,560±5 Ma (using LA-MC-ICPMS), from a tuff bed in the top horizon of the third member of the Gaoyuzhuang Formation in the Yanqing County, northwestern Beijing[8]. Subsequently, Tian et al. (2015) reported a zircon U-Pb age of 1,577±12 Ma from a 15 cm thick tuff in the lower horizon of the third member of the Gaoyuzhuang Formation in Dongshuichang Village, Jixian County[7]. Therefore, the boundary age between the Gaoyuzhuang Formation and the underlying Dahongyu Formation can be dated to ~1,600 Ma, which is coeval with the boundary age between the Statherian and Calymmian. Meanwhile, it can be concluded that the depositional age of the Gaoyuzhuang Formation spans 1,600-1,550 Ma[7,8]. Su et al. (2010) and Li et al. (2014) recognized tuff beds near the base of the second member of the Tieling Formation in northeast of Beijing and the Jixian Section, with zircon U-Pb ages of 1,437±21 Ma[17] and 1,439±14 Ma[18], respectively. A series of age data for the tuff beds in the third member of the Xiamaling Formation, including 1,368±12 Ma[19], 1,370±11 Ma[16], 1,379±12 Ma and 1,380±36 Ma[20], and 1,372±18 Ma[17], have subsequently been reported. In addition, Li et al. (2009) obtained a baddeleyite U-Pb age of 1,320±6 Ma from diabase sills in the Xiamaling Formation[21]. These data assign a reasonably precise boundary age of 1,400 Ma between the Tieling Formation and the overlying Xiamaling Formation, corresponding to the boundary age between the Calymmian and Ectasian. Meanwhile, deposition of the Xiamaling Formation has been identified to span 1,400-1,320 Ma[6,21].

Supplementary Note 2: Samples and sedimentary facies

Samples analyzed in this paper were collected from the Gaoyuzhuang Formation of the Jixian Section. Weathered surfaces were firstly removed and the remaining rock was rinsed with deionized water. Sample powders were obtained from the areas where the matrix was free from veins, disruption and later-stage cements using diamond-tipped drills. Concentrations of Ca and Mg in bulk carbonate rocks were measured with an X-Ray Fluorescence Spectrometer for carbonate content estimation.

The Gaoyuzhuang Formation (~1,600-1,550 Ma) consists mainly of dolostone and limestone deposited in marine environments ranging from supratidal to distal facies[22,23]. The formation shows uncomformable contacts with the underlying Dahongyu Formation and the overlying Yangzhuang Formation, with a thickness of ca. 1,543 m in the Jixian Section. From the base, the Gaoyuzhuang Formation can be divided into four lithological members. The first member, the Guandi Member (315 m), consists mainly of siliceous dolomicrite, microbial dolomicrite, stromatolitic dolomicrite and dolomicrite with minor sandstone, with ca. 3 m thickness of quartz sandstone with ripple-marks on the surface at the bottom of this member (Supplementary Fig. 2a-c), suggesting largely supratidal-intertidal environments[24]. The second member, the Sangshu'an Member (245 m), is composed mainly of thinly bedded clayey dolomicrite, dolomitic siltstone in the lower part (Supplementary Fig. 2d), and moderately thick to thick dolostone in the upper part, representing deposition mainly in a subtidal zone[23]. The third member, the Zhangjiayu Member (706 m), consists mainly of limestone and dolomitic limestone, with a small amount of dolostone and limey dolostone. The nodular limestone, thinly bedded muddy limestone, finely laminated carbonate and black shale in the lower part of the third member (Supplementary Fig. 2e-h) reflect deeper-water environments which may have been below storm wave base[22,23]. A brief regression is recorded in the upper interval of the third member[22,25]. Molar tooth limestone, which generally forms in a slope-subtidal zone, exists in this interval (Supplementary Fig. 2j). The fourth member, the Huanxiusi Member (277 m), mainly comprises bituminous lamellar dolostone, dolomitic micrite and dolosparite in the lower part (Supplementary Fig. 2k), and dolostones containing cherty nodules or beds in the upper part (Supplementary Fig. 2l), which are thought to be deposited mainly in a subtidal-intertidal zone[22,26]. Overall, the epeiric sea in the Yanliao Basin experienced brief transgression-regression cycles with short-term variation in seawater level during the Gaoyuzhuang Period, and sea level reached its highest around the middle part of the Gaoyuzhuang Formation[22,23] (Fig. 1, main text).

Supplementary Note 3: Rare earth element data

Element concentrations in carbonate components can be obtained by dividing the masses of these elements in the selected leachate by the corresponding weight of ($CaCO_3$+$MgCO_3$), which is calculated based on the Ca and Mg contents in the same leachate. The rare earth elements are then normalized to Post-Archean Australian Shale (PAAS)[27] (Fig. 1a, main text). Ce anomaly values (Ce_N/Ce_N^*; where Ce_N refers to observed PAAS-normalized Ce abundance, and Ce_N^* refers to predicted PAAS-normalized Ce concentration) may be calculated in a number of ways, but classically by interpolating from the immediately neighbouring elements La and Pr, as shown below for a simple case:

$$\lg Ce_N^* = (\lg La_N + \lg Pr_N)/2, \text{ that is, } Ce_N^* = (La_N \times Pr_N)^{1/2}$$

$$\text{Thus, } Ce_N/Ce_N^* = Ce_N/ (La_N \times Pr_N)^{1/2} \qquad \text{Eq (1)}$$

Some marine samples are, however, characterized by a positive La anomaly, and thus an artificially large Ce anomaly may arise from an overabundance of La. Where this is the case, the predicted normalized La concentration (La_N^*) can first be calculated by extrapolation from Pr and Nd ($La_N^* = Pr_N \times (Pr_N/Nd_N)^2$; ref 28), and then the Ce anomaly is calculated using this estimate of La_N^*:

$$Ce_N/Ce_N^* = Ce_N/ (La_N^* \times Pr_N)^{1/2}$$

$$= Ce_N/ (Pr_N^3/ Nd_N^2 \times Pr_N)^{1/2}$$

$$= Ce_N/ (Pr_N^2/ Nd_N) \qquad \text{Eq (2)}$$

For GYZ-1 and GYZ-2 samples, there are no obvious La and Ce anomalies in their PAAS-normalized REE patterns (Fig. 1a, main text). Therefore, Ce anomalies were calculated via Eq (1), which gives no discernable calculated Ce anomaly, consistent with the REE trends in Fig. 1b (main text). Furthermore, taking an alternative approach that utilises PAAS-normalized Pr_N/Pr_N^* ($Pr_N/(0.5Ce_N + 0.5Nd_N)$) versus Ce_N/Ce_N^* ($Ce_N/(0.5La_N + 0.5Pr_N)$) after ref 9 (Supplementary Fig. 3) gives the same result. For samples above GYZ-1 and GYZ-2 in the succession, we took the more conservative approach of calculating Ce anomalies via Eq (2) in order to avoid quantifying an artificially large Ce anomaly due to a positive neighbouring La anomaly[28].

Anomalies for Eu and Gd were obtained using Eq (3) and Eq (4), respectively[28]:

$$Eu_N/Eu_N^* = Eu_N/ (Sm_N^2 \times Tb_N)^{1/3} \qquad \text{Eq (3)}$$

$$Gd_N/Gd_N^* = Gd_N/ (Tb_N^2 \times Sm_N)^{1/3} \qquad \text{Eq (4)}$$

The fractionation between LREE and HREE was calculated by the Pr_N/Er_N ratio as per ref 28.

3.1 GYZ-1

For GYZ-1, the REE concentrations vary from 19.87 ppm to 43.56 ppm, with an average of 27.59 ppm. The PAAS-normalized REE distribution patterns are characterized by: (1) MREE or LREE enrichment with Pr_N/Er_N ratios 1.18-1.74 (~1.37 on average); (2) no Ce anomalies; (3) slightly positive Gd anomalies with Gd_N/Gd_N^* 1.05-1.21 (~1.11 on average); (4) near-chondritic Y/Ho ratios of 25.97-28.87 (~27.45 on average).

3.2 GYZ-2

For GYZ-2, the REE concentrations vary from 31.08 ppm to 46.24 ppm, with an average of 39.71 ppm. The REE distribution patterns are characterized by: (1) slightly LREE enrichment with Pr_N/Er_N ratios from 1.05 to 1.31 (~1.17 on average); (2) no Ce anomalies; (3) slightly positive Gd anomalies with Gd_N/Gd_N^* 1.16-1.19 (~1.17 on average); (4) slightly higher Y/Ho ratios of 32.02-33.10 (~32.58 on average).

3.3 GYZ-3

The REE characteristics of carbonates in GYZ-3 could be grouped into three categories approximately based on their PAAS-normalized REE patterns which change from LREE enrichment to nearly flat shape then to consistent LREE depletion from the bottom up (Fig. 1a, main text). Meanwhile, the negative Ce anomaly becomes relatively obvious and the Y/Ho ratio increases to super-chondritic Y/Ho value upwards. In the first group (GYZ-3-1), the REE concentrations vary from 15.49 ppm to 80.94 ppm (~44.94 ppm on average). The REE distribution patterns are characterized by: (1) LREE enrichment with Pr_N/Er_N ratios from 1.09 to 1.90 (~1.53 on average); (2) positive or nearly no La anomalies with La_N/La_N^* 0.92-2.25 (~1.36 on average); (3) no or slightly negative Ce anomalies with Ce_N/Ce_N^* 0.84-1.01 (~0.92 on average); (4) slightly positive Gd anomaly with Gd_N/Gd_N^* 1.23-1.37 (~1.29 on average); (5) slightly higher Y/Ho ratios of 36.12-51.47 (~41.61 on average). The second group (GYZ-3-2) shows variable REE patterns, some of which start to show REE patterns and negative Ce anomalies typical of oxic seawater. Their REE concentrations vary from 35.86 ppm to 104.73 ppm (~65.89 ppm on average). Their REE patterns exhibit: (1) LREE depletion or nearly flat shapes with Pr_N/Er_N ratios 0.62-1.00 (~0.76 on average); (2) slightly positive or nearly no La anomalies with La_N/La_N^* 0.95-1.79 (~1.22 on average); (3) slightly or no negative Ce anomalies with Ce_N/Ce_N^* from 0.79-0.90 (~0.86 on average); (4) slightly positive Gd anomalies with Gd_N/Gd_N^* 1.13-1.28 (~1.20 on average); (5) slightly higher Y/Ho ratios of 37.66-48.54 (~43.74 on average). For the third group (GYZ-3-3), the REE concentrations vary from 21.01 ppm to 91.09 ppm (~49.26 ppm on average). They show consistent typical oxic marine REE patterns with: (1) LREE depletion with Pr_N/Er_N ratios from 0.42-0.83 (~0.63 on average); (2) slightly positive or nearly no La anomalies with La_N/La_N^* 0.94-1.57 (~1.17 on average); (3) negative Ce anomalies with Ce_N/Ce_N^* 0.79-0.92 (~0.85 on average); (4) slightly positive Gd anomalies with Gd_N/Gd^*_N 1.10-1.26 (~1.17 on average); (5) super-chondritic Y/Ho ratios of 39.42-55.76 (~46.87 on average).

3.4 GYZ-4

Samples in GYZ-4 have very low REE concentrations ranging from 1.81 ppm to 3.43 ppm (~2.40ppm on average). They exhibit typical oxic marine PAAS-normalized REE patterns with: (1) LREE depletion with Pr_N/Er_N 0.27-0.50 (~0.37 on average); (2) slightly positive or nearly no La anomalies with La_N/La^*_N 0.90-1.21 (~1.10 on average); (3) negative Ce anomalies with Ce_N/Ce^*_N 0.69-0.86 (~0.81 on average); (4) slightly positive Gd anomalies with Gd_N/Gd^*_N 1.04-1.21 (~1.13 on average); (5) super-chondritic Y/Ho ratios of 44.89-56.46 (~51.58 on average).

Supplementary Note 4: Evaluation of diagenetic alteration and weathering

Diagenetic alteration must be evaluated on sedimentary rocks prior to the interpretation of geochemical data. Petrographic analysis can provide a first-order assessment. Most samples analyzed in this paper are dolomitized, micritic carbonates (Supplementary Fig. 4a-b), or those with a dominantly micritic matrix with distributed small, non-interlocked, euhedral or subhedral replacive dolomites (Supplementary Fig. 4c). Some dolomitised packstones are also noted (Supplementary Fig. 4a). Under cathodoluminescence, packstones show the preservation of original grains without widespread recrystallization. The micrite is usually non-luminescent. Most grains and small, replacive dolomite crystals have a dull luminescent core and bright luminescent rim (Supplementary Fig. 4e-g). Both features suggest very early dolomitization. By contrast, some samples from GYZ-4 show unimodal, nonplanar texture (Supplementary Fig. 4d) which may indicate later, probably deep burial dolomitization, even though they have typical oxic seawater-like REE patterns (Fig. 1a, main text). The possibility of the addition of significant external iron during late diagenesis can be excluded due to their low Fe concentrations (Fe_T<0.5 wt%), and Fe speciation was not undertaken on these samples.

Oxidative weathering of outcrop samples can also mask Fe_{py} enrichments[29]. However, the highly reactive iron pool in these samples is dominated by iron carbonate (Fe_{carb}/Fe_{HR} = 24%-96%, ~69% on average), arguing against a significant influence from weathering.

Inorganic carbon isotopes ($\delta^{13}C_{carb}$) are generally conserved in whole-rock samples of Proterozoic carbonates due to a low water/rock ratio for carbon during the interaction with diagenetic and/or post-diagenetic fluids[30]. $\delta^{18}O_{carb}$ values are more sensitive to diagenetic processes as meteoric fluids are commonly characterized by lighter $\delta^{18}O$ values than seawater[31]. Generally, carbonates with $\delta^{18}O_{carb}$>-10‰ are considered to preserve primary $\delta^{13}C_{carb}$ values[32]. In our study, the $\delta^{18}O_{carb}$ values of the Gaoyuzhuang carbonates in the Jixian Section are all greater than -8‰. Moreover, there is lack of correlation between the $\delta^{13}C_{carb}$ and $\delta^{18}O_{carb}$ values (Supplementary Fig. 6). Therefore, the $\delta^{13}C_{carb}$ data presented in this paper primarily reflect contemporaneous seawater signatures.

References

1. Lu, S., Yang, C., Li, H. & Li, H. A group of rifting events in the terminal Paleoproterozoic in the North China Craton. *Gondwana Research* **5,** 123-131 (2002).
2. Zhu, S. et al. Decimetre-scale multicellular eukaryotes from the 1.56-billion-year-old Gaoyuzhuang Formation in North China. *Nat Commun* **7,** 11500 (2016).
3. Guo, H. et al. Isotopic composition of organic and inorganic carbon from the Mesoproterozoic Jixian Group, North China: Implications for biological and oceanic evolution. *Precambrian Research* **224,** 169-183 (2013).
4. Li, R., Chen, J., Zang, S. & Chen, Z. Secular variations in carbon isotopic compositions of carbonates from Proterozoic successions in the Ming Tombs Section of the North China Platform. *Journal of Asian Earth Sciences* **22,** 329-341 (2003).
5. Gao, L. et al. Detrital zircon dating of Meso- and Neoproterozoic rocks in North China and its implications. *Acta Geologica Sinica (English Edition)* **85,** 271-282 (2011).
6. Li, H. et al. Recent advances in the study of the Mesoproterozoic geochronology in the North

China Craton. *Journal of Asian Earth Sciences* **72,** 216-227 (2013).

7. Tian, H. et al. Zircon LA-MC-ICPMS U-Pb dating of tuff from Mesoproterozoic Gaoyuzhuang Formation in Jixian Country of North China and its geological significance. *Acta Geoscientica Sinica* **36,** 647-658 (2015).
8. Li, H. et al. Further constraints on the new subdivision of the Mesoproterozoic stratigraphy in the northern North China Craton. *Acta Petrologica Sinica* **26,** 2131-2140 (2010).
9. Bau, M. & Dulski, P. Distribution of ytttium and rare-earth elements in the Penge and Kuruman iron-formations, Transvaal Supergroup, South Africa. *Precambrian Research* **79,** 37-55 (1996).
10. Zhao, G., Sun, M., Wilde, S. A. & Li, S. A Paleo-Mesoproterozoic supercontinent: assembly, growth and breakup. *Earth-Science Reviews* **67,** 91-123 (2004).
11. Huang, X. Tectonic evolution of the Meso-Neoproterozoic sedimentary basin in Yanshan Range. *Geological Survey and Research* **29,** 263-270 (2006).
12. Meng, X. & Ge, M. Research on cyclic sequence, events and formational evolution of the Sino-Korea plate. *Earth Science Frontiers* **9,** 125-140 (2002).
13. Li, H. et al. The base age of the Changchengian System at the northern North China Craton should be younger than 1670Ma: Constraints from zircon U-Pb LA-MC-ICPMS dating of agranite-porphyry dike in Miyun County, Beijing. *Earth Science Frontiers* **18,** 108-120 (2011).
14. Lu, S. & Li, H. A precise U-Pb single zircon age determination for the volcanics of Dahongyu Formation, Changcheng System in Jixian. *Bulletin of the Chinese Academy of Geological Sciences* **22,** 137-146 (1991).
15. Lu, S., Zhao, G., Wang, H. & Hao, G. Precambrian metamorphic basement and sedimentary cover of the North China Craton: A review. *Precambrian Research* **160,** 77-93 (2008).
16. Gao, L. et al. SHRIMP zircon ages: Basis for refining the chronostratigraphic classfication of

the Meso- and Neoproterozoic strata in North China old land. *Acta Geologica Sinica* **29,** 366-376 (2008).

17. Su, W. et al. SHRIMP U-Pb dating for a K-bentonite bed in the Tieling Formation, North China. *Chinese Science Bulletin* **55,** 3312-3323 (2010).
18. Li, H. et al. The first precise age constraints on the Jixian System of the Meso-Neoproterozoic standard section of China: SHRIMP zircon U-Pb dating of bentonites from the Wumishan and Tieling Formations in the Jixian Section, North China Craton. *Acta Petrologica Sinica* **30,** 2999-3012 (2014).
19. Gao, L., Zhang, C., Shi, X., Zhou, H. & Wang, Z. Zircon SHRIMP U-Pb dating of the tuff bed in the Xiamaling Formation of the Qingbaikouan System in North China. *Geological Bulletin of China* **26,** 249-255 (2007).
20. Su, W. et al. SHRIMP U–Pb ages of K-bentonite beds in the Xiamaling Formation: Implications for revised subdivision of the Meso- to Neoproterozoic history of the North China Craton. *Gondwana Research* **14,** 543-553 (2008).
21. Li, H. et al. Zircon and beddeleyite U-Pb precision dating of basic rock sills intruding Xiamaling Formation, North China. *Geological Bulletin of China* **28,** 1396-1404 (2009).
22. Mei, M. Preliminary study on sequence-stratigraphic position and origin for Molar-tooth structure of the Gaoyuzhuang Formation of Mesoproterozoic at Jixian section in Tianjin. *Journal of Palaeogeography* **7,** 437-447 (2005).
23. Guo, H. et al. Sulfur isotope composition of carbonate-associated sulfate from the Mesoproterozoic Jixian Group, North China: Implications for the marine sulfur cycle. *Precambrian Research* **266,** 319-336 (2015).
24. Seong-Joo, L. & Golubic, S. Microfossil populations in the context of synsedimentary micrite deposition and acicular carbonate precipitation: Mesoproterozoic Gaoyuzhuang Formation, China. *Precambrian Research* **96,** 183-208 (1999).

25. Mei, M. Sedimentary features and their implication for the depositional succession of non-stromatolitic carbonates, Mesoproterozoic Gaoyuzhuang Formation in Yanshan area of North China. *Geoscience* **21,** 45-56 (2007).

26. Tang, D., Shi, X., Wang, X. & Jiang, G. Extremely low oxygen concentration in mid-Proterozoic shallow seawaters. *Precambrian Research* **276**, 145-157 (2016).

27. Taylor, S.R. & McLennan, S.M. *The Continental Crust: Its Composition and Evolution*. (Blackwell Scientific Publications, Oxford, 1985).

28. Lawrence, M. G. & Kamber, B. S. The behaviour of the rare earth elements during estuarine mixing-revisited. *Marine Chemistry* **100,** 147-161 (2006).

29. Clarkson, M. O., Poulton, S. W., Guilbaud, R. & Wood, R. A. Assessing the utility of Fe/Al and Fe-speciation to record water column redox conditions in carbonate-rich sediments. *Chemical Geology* **382,** 111-122 (2014).

30. Knoll, A. H., Hayes, J. M., Kaufman, A. J., Swett, K. & Lambert, I. B. Secular variation in carbon isotope ratios from Upper Proterozoic successions of Svalbard and East Greenland. *Nature* **321,** 832-838 (1986).

31. Veizer, J. & Hoefs, J. The nature of O^{18}/O^{16} and C^{13}/C^{12} secular trends in sedimentary carbonate rocks. *Geochimica et Cosmochimica Acta* **40,** 1387-1395 (1976).

32. Kaufman, A. J. & Knoll, A. H. Neoproterozoic variations in the C-isotopic composition of seawater: stratigraphic and biogeochemical implications. *Precambrian Research* **73,** 27-49 (1995).